THERMAL EXPANSION MISMATCH AND OXIDATION IN THERMAL BARRIER COATINGS*

G. C. Chang and W. Phucharoen
Cleveland State University

R. A. Miller
National Aeronautics and Space Administration
Lewis Research Center

INTRODUCTION

Thermal barrier coatings (TBC) for advanced gas turbine blades have been under intensive development during the last several years. This is a very complex problem calling for inter-disciplinary efforts. This particular investigation is intended to help achieve a clearer understanding of the mechanical behavior of plasma-sprayed zirconia-yttria TBCs, involving a nickel-chromium-aluminum bond coat. The near-term objectives of this project is to study the stress states in a relatively simple model TBC subjected to steady-state thermal loading. The resulting thermal expansion mismatch and oxidation have been primary targets for the study.

Due to the complex nature of the problem on hand, the versatile finite element approach has been used to determine the stress states. Preliminary results obtained were discussed in reference 1. This paper describes the finite element approach and the effects of thermal expansion mismatch and oxidation. A proposed mechanism for oxidation-induced coating failure is also presented.

EXPERIMENTAL OBSERVATIONS OF FRACTURING OF COATINGS

Since the late 1970's, a number of researchers have reported their experimental TBC work. While some worked with simple test specimens, others ran tests of full-size engine turbine blades. Of particular interest to the present investigation is the work reported in reference 2. In this particular work, superalloy cylindrical test specimens with a radius of 0.65 cm and a length of 7.60 cm were utilized. The specimens were plasma-spray coated with the zirconia-yttria on a nickel-chromium-aluminum bond coat. Coated specimens were then individually exposed to the combustion gases of a burner rig for various periods of time before cooling took place. Most specimens went through many thermal cycles.

It was reported, in reference 2, that the coatings of all specimens tested in air at temperatures high enough to permit bond coat oxidation eventually spalled. Evidence gathered by both visual inspections and scanning electron microscope (SEM) photomicrograph indicated that such spalling was preceded by coating delamination. The TBC specimens failed within the ceramic coat just above the bond coat on cooling from high temperatures. The same photomicrography also showed the rough interface between the ceramic layer and the bond coat. Some interfaces were roughly sinusoidal with peak-to-valley and peak-to-peak dimensions up to 50-100 micrometers (μm). Furthermore, oxides had been found in the bond coat adjacent to the ceramic-bond interface. Much oxides accumulated through thermal-exposure of these specimens in the air.

*Work performed under Cooperative Research Agreement No. NCC-3-27.

These test results clearly illustrated the failure modes. They also raised the question of the quantitative nature of the stress states which may have some bearing on the TBC failure mechanism(s). This then led to the present investigation.

FINITE ELEMENT MODELING OF A BASIC THERMAL BARRIER COATING

Based on the above experimental observations and the need to understand the detailed distribution of stresses and strains within the TBC, it was decided that a general-purpose finite element program be used to model a cylindrical test specimen similar to that reported in reference 2. Figure 1 illustrates this modeling concept.

The cylinder is sufficiently long, as compared to its diameter, that the problem can be approximated by a two-dimensional generalized plane-strain case. Such an approximation, which can often be found in the classical theory of elasticity, implies that the strain in the axial (or z) direction is constant for any unit slice such as the one shown in figure 1.

A wavy interface between the bond and the ceramic coat is introduced, with a period as well as peak-to-valley amplitude of 50 μm (0.002 in.). This and other geometric dimensions of the wedge modeled are shown in figure 2.

The three materials comprising the substrate, the bond coat, and the ceramic layer, are assumed, for the time being, to be homogeneous, isotropic and linearly elastic. Each material, naturally, possesses its own temperature-dependent parameters, such as Young's modulus (E), Poisson's ratio (ν), and thermal expansion coefficient (α). This greatly simplified material model represents a first step toward obtaining a detailed solution to a complex TBC problem on hand. Nevertheless, more complex models such as plasticity, viscoelasticity or creep, etc., would be incorporated in future calculations.

An overview of the advanced "TBCOC" model is given in figure 3. The model consists of 1316 nodal points and 2140 plane-strain finite elements, both triangular and quadrilateral. Particular attention has been given to the region in the vicinity of the sinusoidal interface in the discretization process. Details of that portion of the model of principal interest are shown in figures 4 to 11. Oxidized elements shown in figures 3, 8 and 9, are special types of bond coat elements. The actual modeling is done with the use of a general purpose computer program known as MARC (ref. 3) which is operational on a supercomputer (CRAY-I) at NASA Lewis Research Center.

The boundary conditions applied are fully compatible with those normally required in the theory of elasticity. More specifically, only radial displacements are allowed to occur along radial lines, OA and OB, in figures 2 and 3. Line AB is free to displace. Point O which represents the center of the unit slice or the z-axis of the cylindrical specimen, is fixed.

To validate the finite element solution, the TBCOC solution to a limiting case has been obtained. In this case, the elements in the ceramic layer and the bond coat have been assigned material properties identically the same as those of the

substrate. The finite element solution matches extremely closely with that of the analytical solution.

STRESS STATES RESULTING FROM THERMAL EXPANSION MISMATCH

The TBCOC computer program has been used to determine stress states for several combinations of TBC material properties. Customary units (psi, in., etc.) have been used in the calculations. The only loading applied so far is one of a uniform temperature drop throughout the model. It simulates part of the cooling-off of a TBC experiencing a temperature drop of 100°C from an assumed stress-free temperature of 700°C. Material properties for three cases are given in Table 1. It should be noted that only values of E, the Young's modulus, have changed from Cases A-2 to A-3 to A-4.

Stresses for Case A-2 are presented in figures 12-14, with corresponding strains shown in figures 15-17. The strains are of reasonable size and distribution. Stresses in the x-direction, or radial stresses, in the vicinity of the sine peak (asperity) are rather high, and are tensile in nature. Such high tensile stresses could easily initiate cracking at the asperities as the TBC cools down. It should be pointed out that these stresses correspond to a 100°C drop in temperature. An additional temperature drop would produce higher tensile stresses yet. There should be little doubt that cracking could be initiated at the asperities at some point during the cooling process. This is especially convincing when one recalls that the occurence of such cracking may contribute to the accoustic emission observed as thermal barrier coated specimens cool (ref. 4). This is the first major observation of this work.

The stresses in the y-direction, or hoop stresses, as shown in figure 13, are in compression, as expected. These stresses are fairly uniform throughout the thickness of the coating. Shearing stresses shown in figure 14, however, maximize near the interface where failure is observed. It is inappropriate to make any conclusive remarks about these two stresses due to lack of reliable data on allowable stresses for this ceramic material at the present time.

Case A-3 employs a value of E which is half of that of Case A-2. From an elasticity viewpoint, the lower E value would allow more deformation in ceramic layer, resulting in lower stresses in all directions. This indeed occurred, as evidenced by the data shown in figures 18-20. Such is observation no. 2. It is noted that peak stresses went down by nearly 40 percent in the x-direction.

A third observation is that from an elasticity viewpoint, a softer bond coat with a lower E tends to lower stresses in the ceramic layer. This is the result by comparing figures 12-14 with 21-23. The reduction in peak stress caused by decreasing the bond coat modulus by a factor of two is on the order of 10 percent, making it much less significant than a comparable change in the modulus of the ceramic layer.

A comparison between the plane-strain finite element results and the results of more approximate calculations is in order. The stress in the y-direction in a thin ceramic coating at a planar interface is approximated by (refs. 2 and 5)

$$\sigma_y = \frac{\Delta \alpha \Delta T}{1 - \mu_c} \cdot E_c$$

where $\Delta\alpha$ is the difference in thermal expansion coefficient between the ceramic and the substrate, ΔT is the temperature change, E_c is the modulus of the ceramic, and μ_c is Poisson's ratio. Using values of these properties from Table 1 and treating the substrate as if it were composed entirely of bond coat material yields

$$\sigma_y \text{ (A2)} = \sigma_y \text{ (A4)} = -19.0 \text{ MPa}$$

and

$$\sigma_y \text{ (A3)} = -9.5 \text{ MPa}$$

These values agree well with the peak values of

$$\sigma_y \text{ (A2)} = \sigma_y \text{ (A4)} = -18 \text{ MPa (18.4 MPa)}$$

and

$$\sigma_y \text{ (A3)} = -10 \text{ MPa (-9.3 MPa)}$$

given in figures 13, 19 and 22. Numbers within parentheses are taken from computer printouts and are exact values not shown by contouring.

An expression for the interfacial stress in the direction normal to the sinusoidal interface is given in equation 4 of reference 5. The expression predicts maximum stress at the peaks of the asperities and equally negative stresses in the valleys. Zero stress is predicted midway between peak and valley. Inserting the parameters in Table 1 into equation 4 of reference 5 gives

$$\sigma_x \text{ (A2)} = 16.4 \text{ MPa}$$

$$\sigma_x \text{ (A3)} = 9.1 \text{ MPa}$$

$$\sigma_x \text{ (A4)} = 13.8 \text{ MPa}$$

The values reported in figures 12, 18, and 21 are

$$\sigma_x \text{ (A2)} = 18 \text{ MPa (19.6 MPa)}$$

$$\sigma_x \text{ (A3)} = 10 \text{ MPa (11.3 MPa)}$$

$$\sigma_x \text{ (A4)} = 14 \text{ MPa (15.2 MPa)}$$

The above finite element results and the approximate values agree well. However, the stresses reported in at least one case, figure 21, are not sinusoidal. It appears that the approximate expressions provide a useful and quick view of maximum stresses in the x and y directions, but they are less useful in mapping out the actual stress fields. The finite element technique is also required for obtaining the corresponding strains as well as the shearing stresses and strains.

STRESS STATES DUE TO OXIDATION

In experimental work reported in reference 2, bond coat oxidation was seen to grow with thermal cycles when the test was conducted in the air and failure was found to be correlated with this oxidation. The oxide layer appeared to grow thicker with exposure to the air at high temperatures. The net effect is equivalent to inserting an extra oxide layer between the ceramic layer and the remaining unoxidized bond material. The oxide is largely alumina which is a hard and strong material. As such, the stress state in the ceramic is expected to be severely impacted by the expanding oxide layer.

As a first attempt to model the effects of bond coat oxidation, the single layer of finite elements which border on the sinusoidal interface have been assigned the properties of alumina. These elements are shown by the dark outlines in figures 8 through 11. Oxide growth has been represented by giving these elements an artifically large thermal expansion coefficient given by

$$\alpha_a = G \times \alpha$$

where G is a growth factor. Proper choice of G rests with the need to make sure that the observed thickness of the oxide layer should be approximately equal to the product of α_a and 3 μm. For the present case G was set equal to -1000. A temperature drop of only 0.1°C was used to minimize thermal expansion mismatch stresses. This yielded a very modest expansion of 0.08% in the oxide layer. The resulting stresses due to this oxidation-like process are presented in figures 24-26, Case A-10.

The stresses obtained for Case A-10 are, in general, the reverse of those obtained for Cases A-2 through A-4. Stresses in the x-direction, figure 24, are compressive near the peak of the asperity and tensile above the valley. Stresses in the y-direction, figure 25, are positive near the peak of the asperity while still being negative elsewhere. Shearing stresses, figure 26, are, in general, in the opposite direction (opposite sign).

The magnitude of the above stresses are very large considering that only a very modest expansion of the oxide has been modeled. Therefore, the stress state due to oxidation can be expected to have a profound influence on the coating failure mechanism. In fact, these stresses are so large that the coating system must actually relieve much of the stresses through such processes as bond coat flow (ref. 2), ceramic microcracking, or other inelastic-like effects (ref. 6). Such efforts are not treated in the present linear analysis.

A PROPOSED MECHANISM FOR OXIDATION-INDUCED COATING FAILURE

Based on the analytical results discussed above, a tentative mechanism may be proposed to account for the observed correlation between bond coat oxidation and coating failure. Consider the radial component of stress as indicated in figure 27. Initially, radial stresses at the peaks of the asperities are tensile. This

promotes cracking in the ceramic near the interface in that region. However, such cracks will be restrained from propagating into the region above the valley where the stresses are compressive.

As the coating oxidizes the stress in the region above the valley becomes tensile. Now the cracks may extend. This would eventually lead to delamination and spalling of the ceramic layer.

Work is underway to model the stress fields around this growing crack. Both the initial cracking and the oxidation are being taken into consideration.

CONCLUDING REMARKS

The present investigation represents a modest effort in combining three types of expertise: experimental material research, finite element techniques, and computer science. The authors wish to acknowledge the very significant contributions from the computer science community. Through Dr. James Guptill, of the Computer Services Division at NASA Lewis Research Center, both efficient software systems and powerful computers were brought to bear on the complex problem on hand. To ensure future success, a similar interdisciplinary approach will continue to be employed.

With the TBCOC program now operational, additional data will be generated to gain a clearer understanding of the stress states in not only the ceramic layer but also the bond coat. Shortly, TBCOC will also be used to study the effect of initial cracks in the vicinity of the asperities. Both thermal expansion and oxidation cases will soon be investigated.

The development of another computer model, known as TBCG, is well underway. This model entails a more smooth ceramic-bond interface. With the use of both computer models, a detailed study of the interface geometry will be performed within approximately six months.

The work to date has used linearly elastic material models. This may not be quite realistic. Nevertheless, this approach has made it possible to gain valuable insights into the TBC stress states under varying conditions. Results so obtained are deemed valuable in guiding experimental work as well. As a goal for the future, the present work would logically be extended into the inelastic material regime. The results from such a future cooperative endeavor between the experimentalist and the analyst may prove to be extremely useful indeed.

REFERENCES

1. Chang, G. C. and Phucharoen, W.: Finite Element Analysis of Thermal Barrier Coatings. NASA Workshop on Thermal Barrier Coatings, Middleburg Heights, May 1985.

2. Miller, R. A. and Lowell, C. E.: Failure Mechanism of Thermal Barrier Coatings Exposed to Elevated Temperatures. Thin Solid Films, 95, 1983, pp. 265-273.

3. Anonymous: MARC Finite Element Program User Manual, Version K-1, MARC Analysis Research Corp., 1983.

4. Berndt, Christopher C. and Miller, Robert A.: Failure Analysis of Plasma-Sprayed Thermal Barrier Coatings. NASA Technical Memorandum 83777, 1984.

5. Evans, A. G., Crumley, G. B., and Demaray, R. E.: On the Mechanical Behavior of Brittle Coatings and Layers. Oxidation of Metals, v. 20, Nos. 5/6, 1983.

6. Firestone, R. F., Logan, W. R., Adams, J. W., and Bill, R. C.: Creep of Plasma-Sprayed Zirconium Dioxide Thermal Barrier Coatings. Ceramic Engineering and Science Proceedings, 3, 1982, pp. 158-71.

TABLE 1

MATERIAL PROPERTIES

CASE	MATERIAL	E (MP_a)	ν	ρ (gm/cm^3)	α ($m/m/°C$)
A-2	Ceramic	0.0276×10^6	0.25	5.659	10.01×10^{-6}
	Bond Coat	0.1379×10^6	0.27	6.990	15.16×10^{-6}
	Substrate	0.1758×10^6	0.25	7.767	13.91×10^{-6}
A-3	Ceramic	0.0138×10^6	0.25	5.659	10.01×10^{-6}
	Bond Coat	0.1379×10^6	0.27	6.990	15.16×10^{-6}
	Substrate	0.1758×10^6	0.25	7.767	13.91×10^{-6}
A-4	Ceramic	0.0276×10^6	0.25	5.659	10.01×10^{-6}
	Bond Coat	0.0690×10^6	0.27	6.990	15.16×10^{-6}
	Substrate	0.1758×10^6	0.25	7.767	13.91×10^{-6}
A-10	Ceramic	0.0276×10^6	0.25	5.659	10.01×10^{-6}
	Bond Coat	0.1379×10^6	0.27	6.990	15.16×10^{-6}
	Substrate	0.1758×10^6	0.25	7.767	13.91×10^{-6}
	Oxidized Layer	0.3448×10^6	0.32	3.772	7.79×10^{-3}

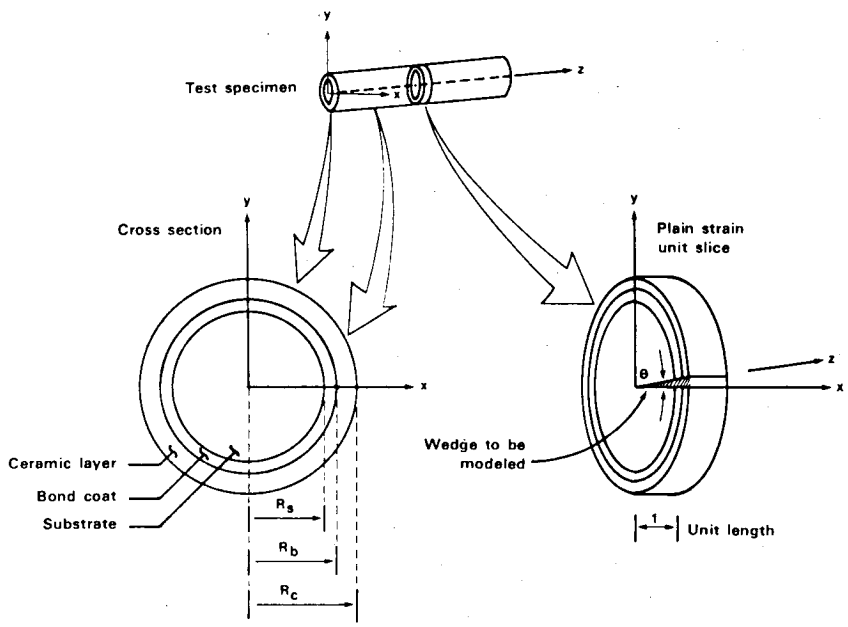

Figure 1. CYLINDRICAL TBC TEST SPECIMEN

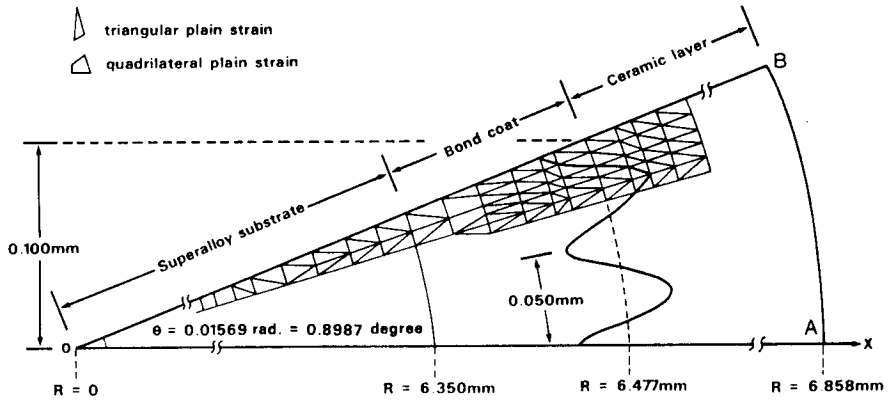

Figure 2. THE TBC FINITE ELEMENT MODEL

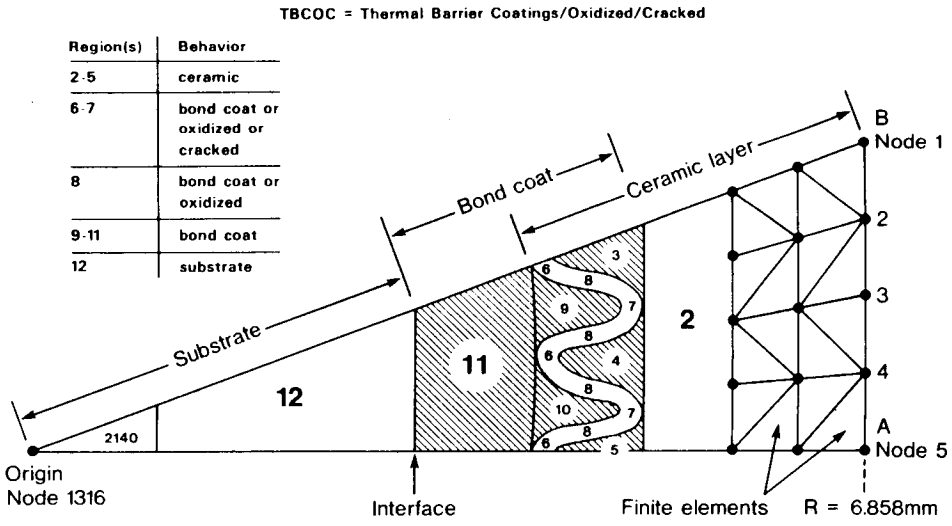

Figure 3. OVERVIEW OF THE ADVANCED TBCOC MODEL

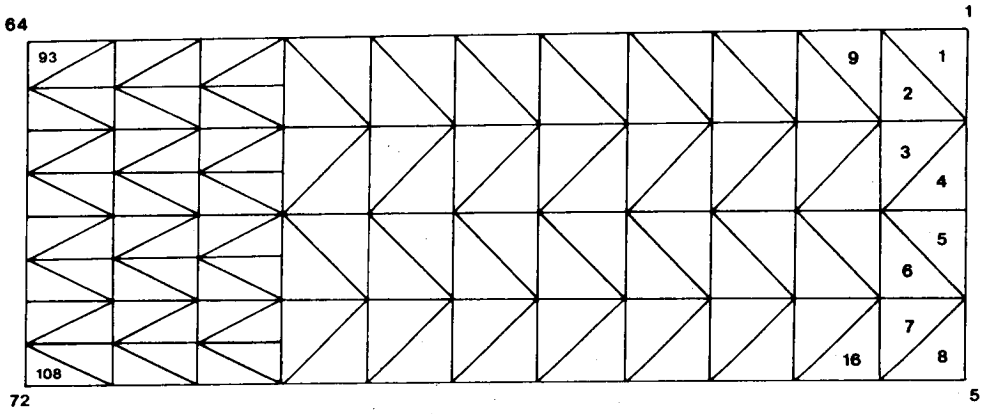

Figure 4. TBCOC MODEL (PART 1)

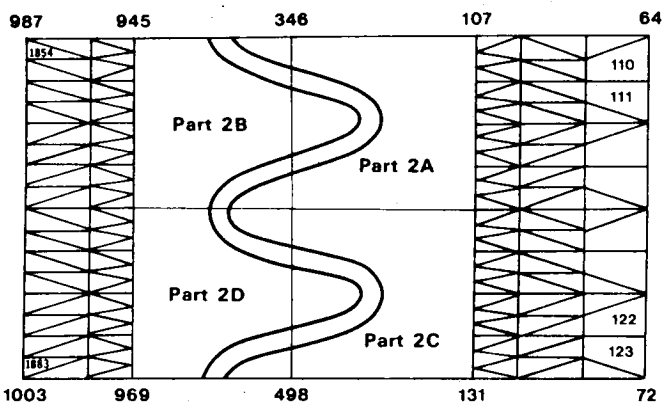

Figure 5. TBCOC MODEL (PART 2)

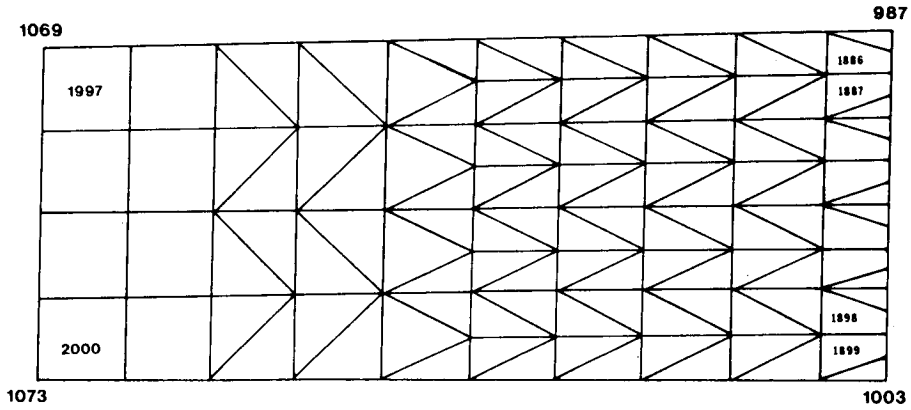

Figure 6. TBCOC MODEL (PART 3)

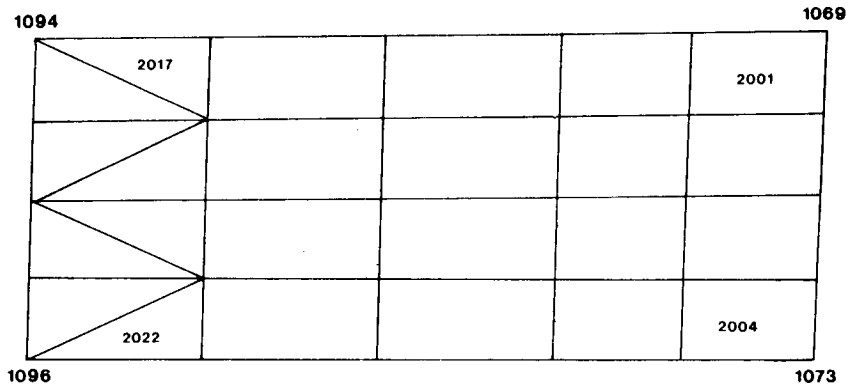

Figure 7. TBCOC MODEL (PART 4)

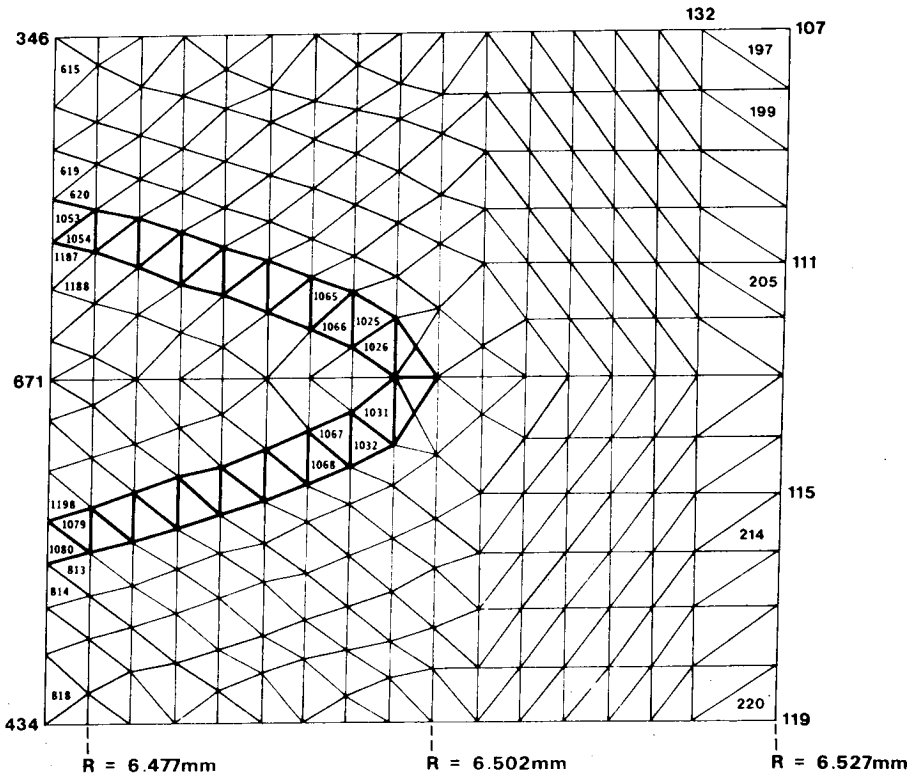

Figure 8. FINITE ELEMENT DETAILS (PART 2A)

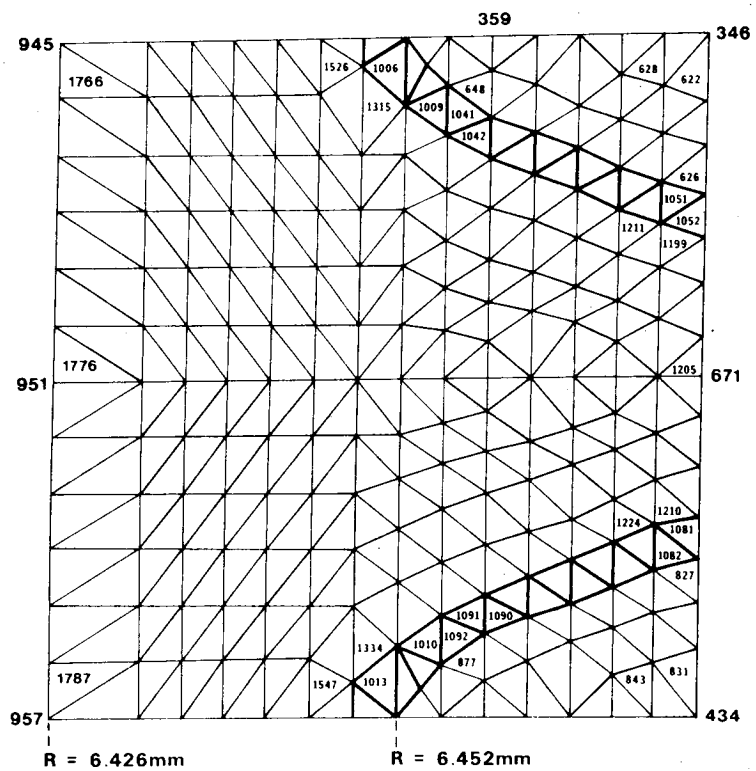

Figure 9. FINITE ELEMENT DETAILS (PART 2B)

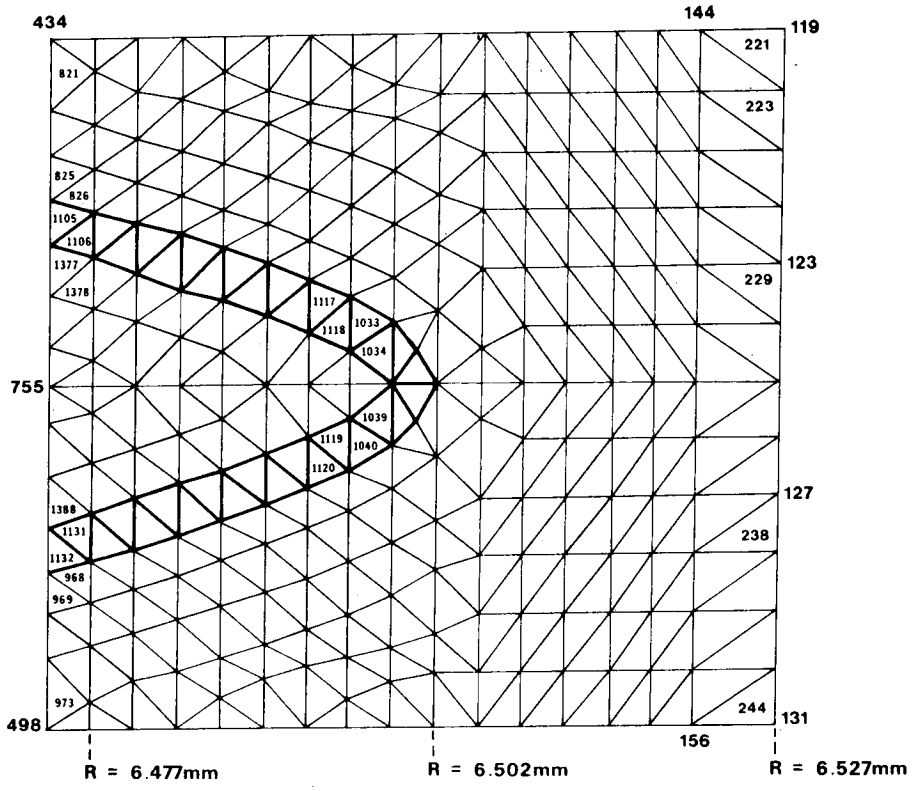

Figure 10. FINITE ELEMENT DETAILS (PART 2C)

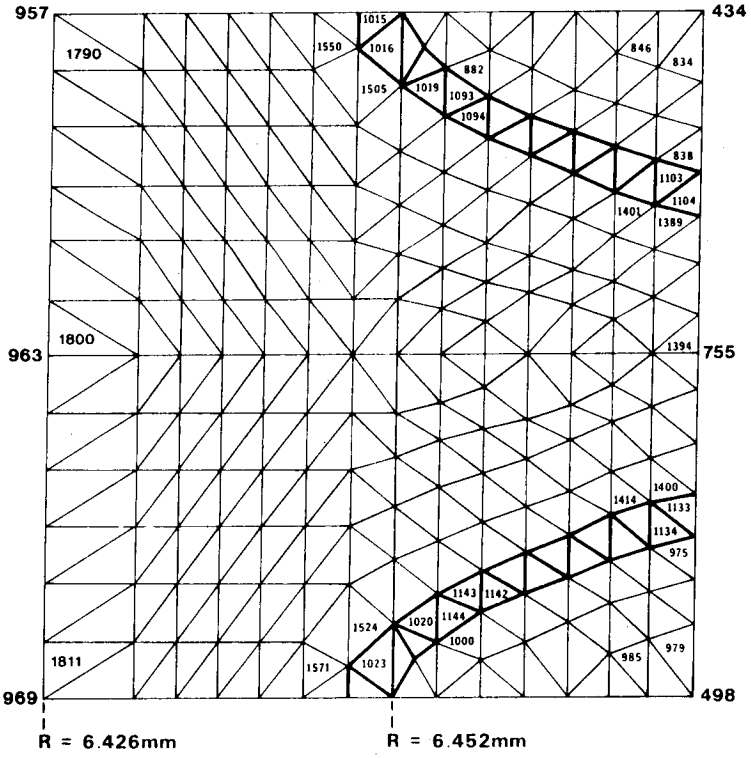

Figure 11. FINITE ELEMENT DETAILS (PART 2D)

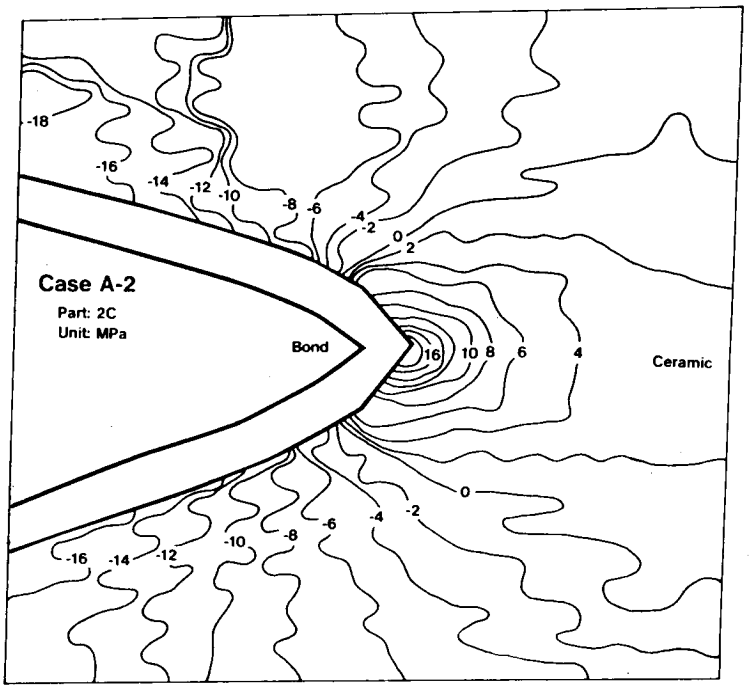

Figure 12. STRESSES IN X - DIRECTION

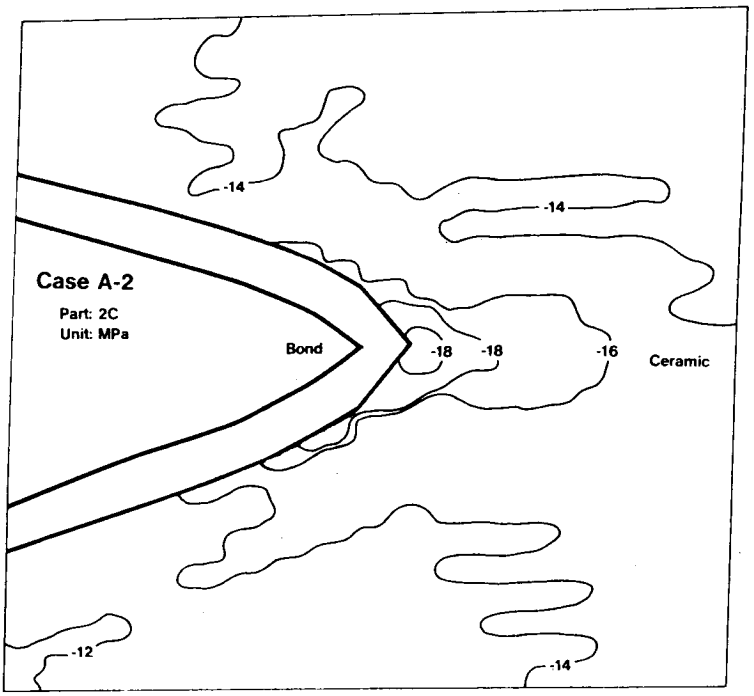

Figure 13. STRESSES IN Y - DIRECTION

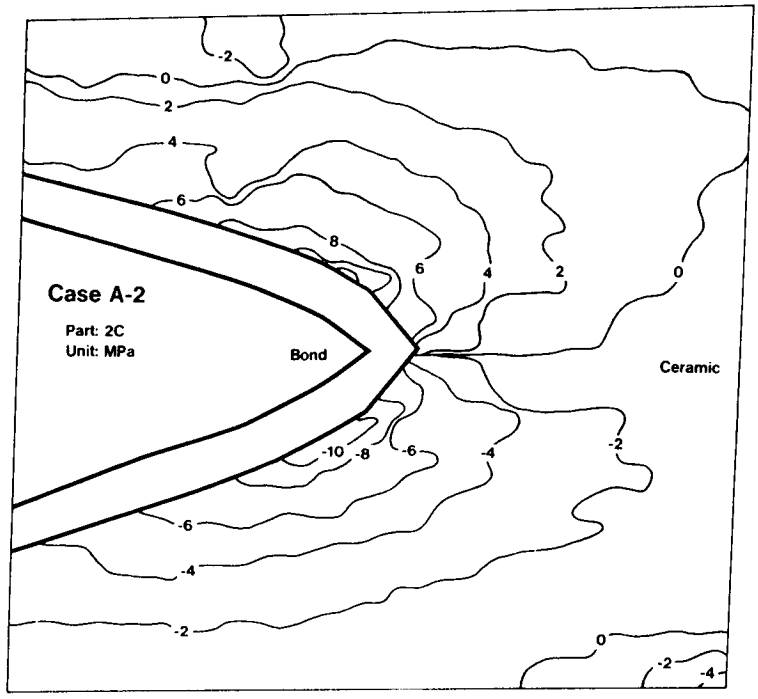

Figure 14. SHEARING STRESSES

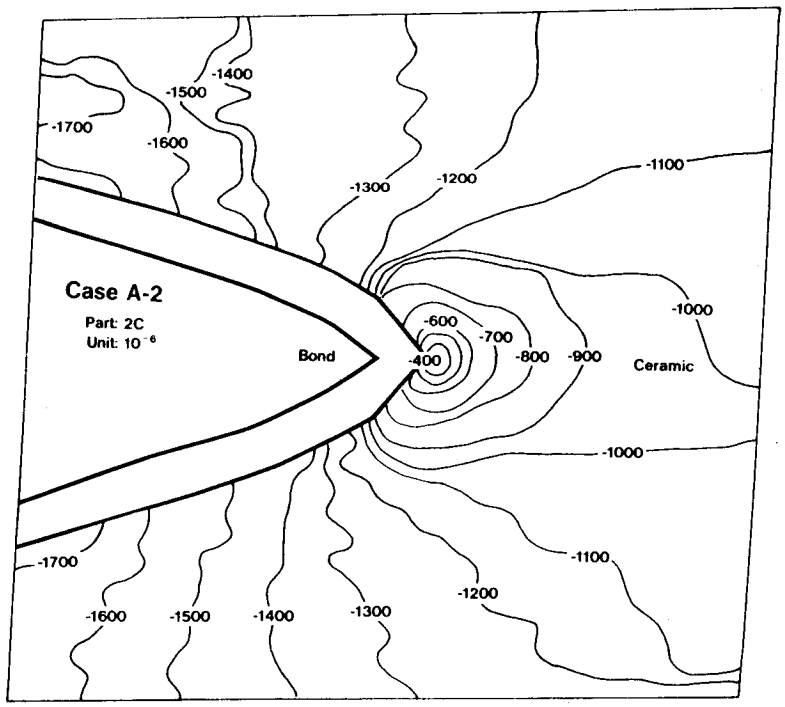

Figure 15. STRAINS IN X - DIRECTION

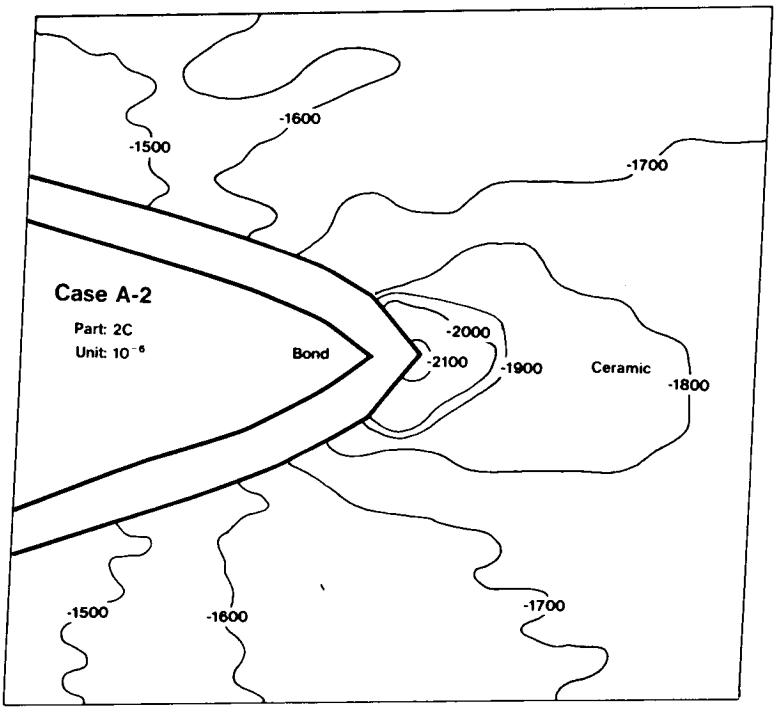

Figure 16. STRAINS IN Y - DIRECTION

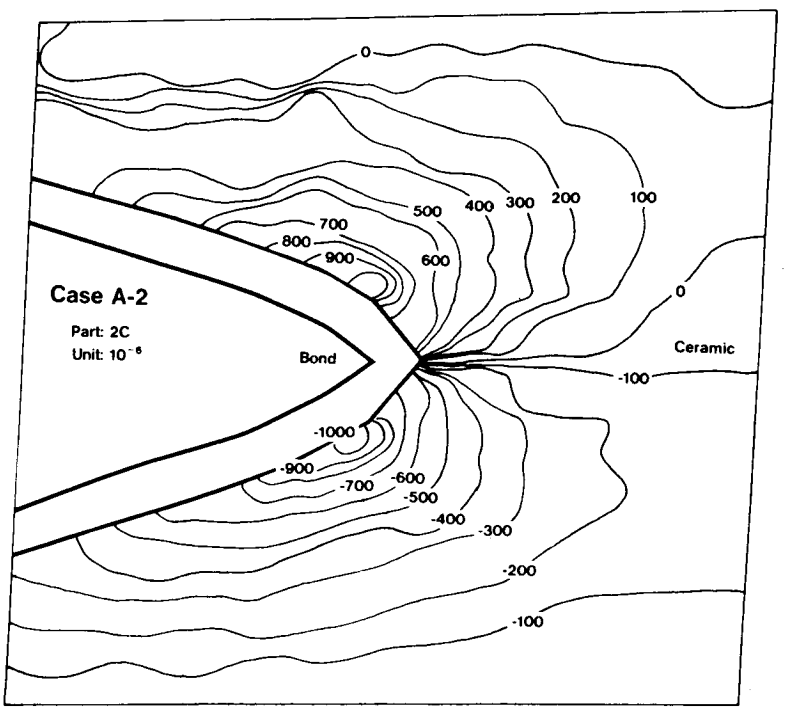

Figure 17. SHEARING STRAINS

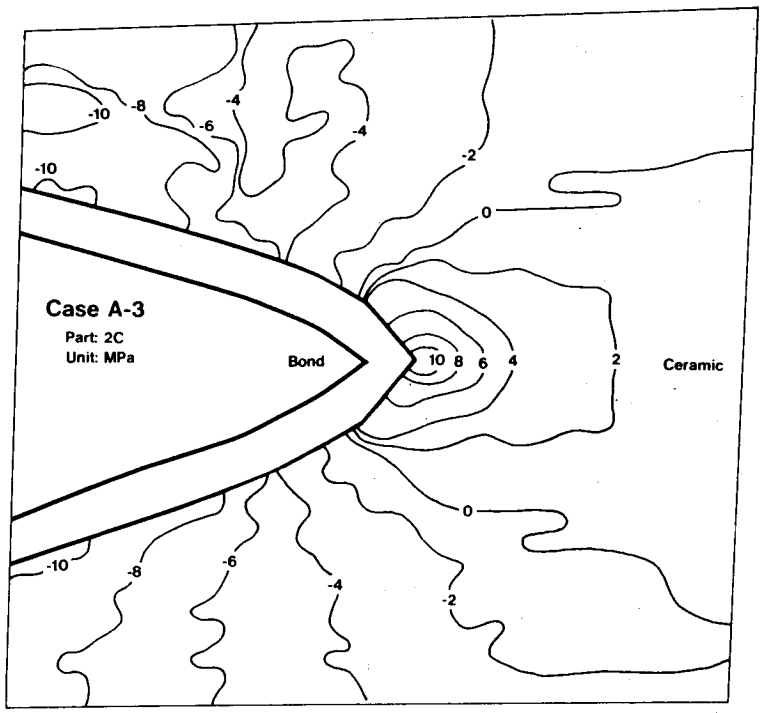

Figure 18. STRESSES IN X - DIRECTION

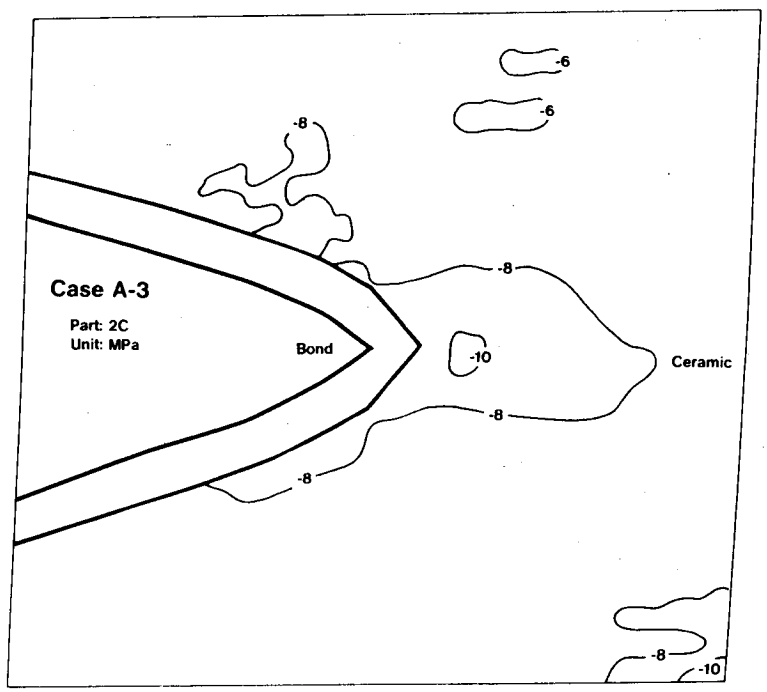

Figure 19. STRESSES IN Y - DIRECTION

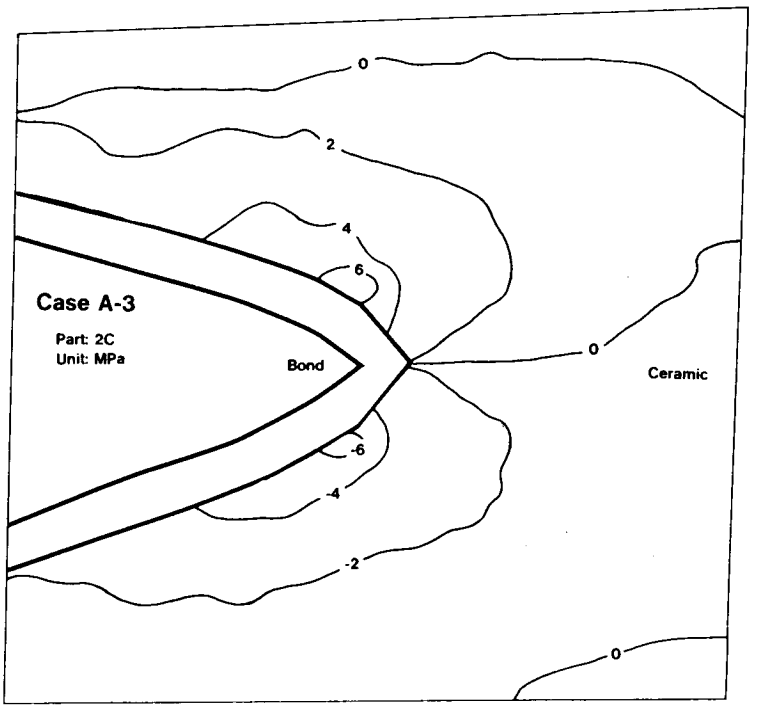

Figure 20. SHEARING STRESSES

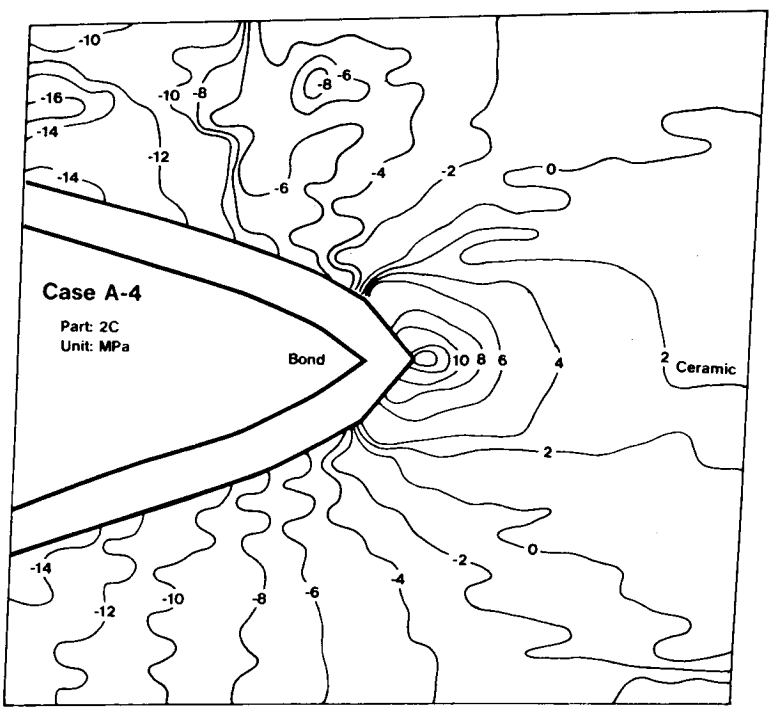

Figure 21. STRESSES IN X - DIRECTION

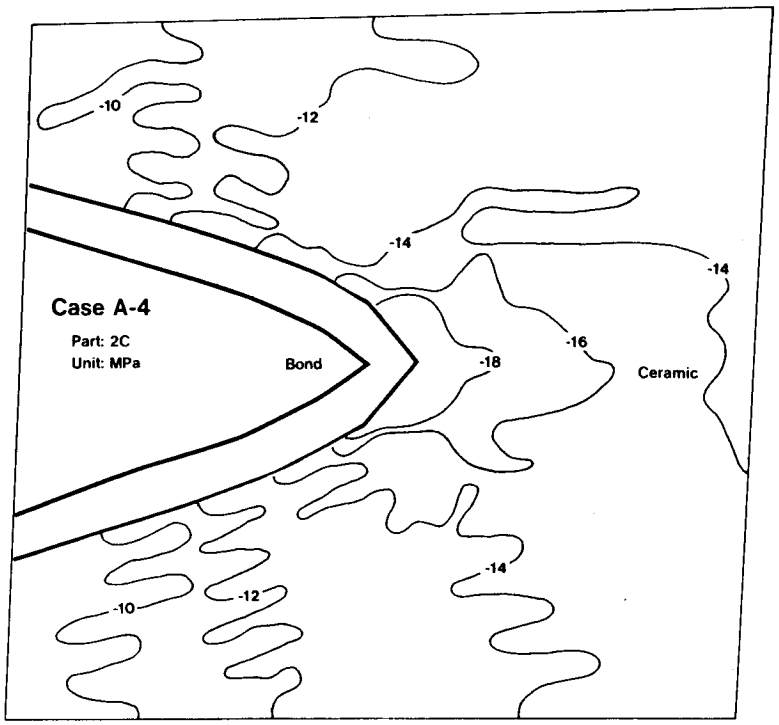

Figure 22. STRESSES IN Y - DIRECTION

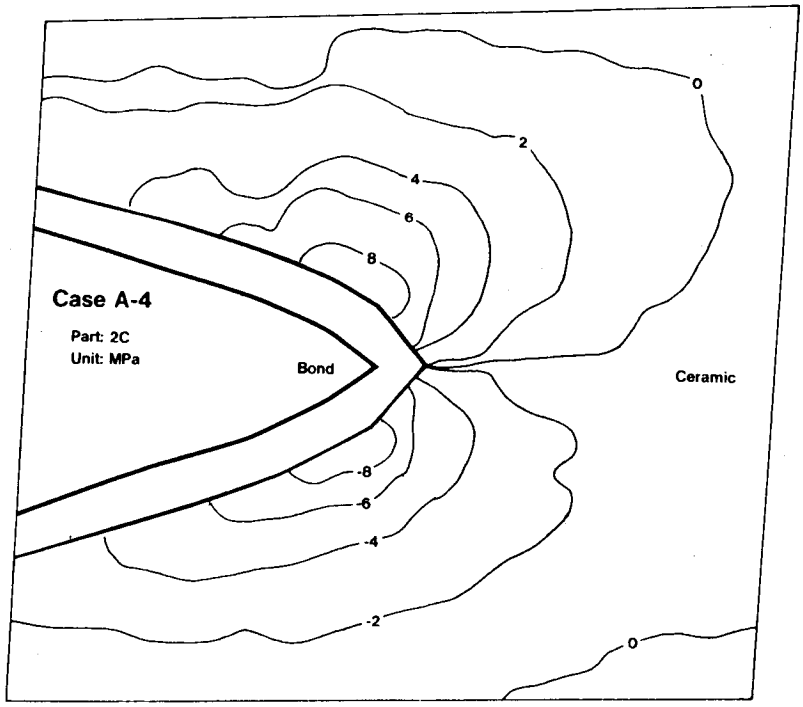

Figure 23. SHEARING STRESSES

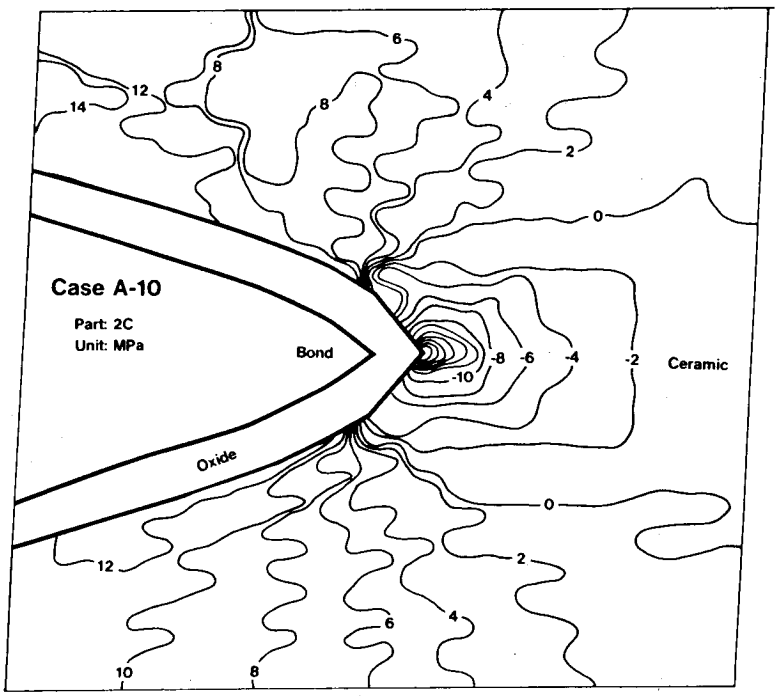

Figure 24. STRESSES IN X - DIRECTION

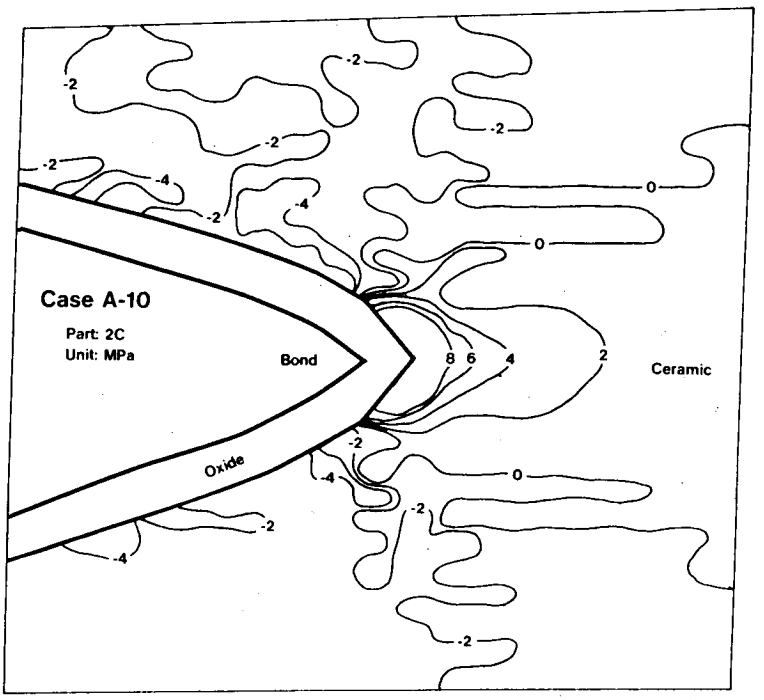

Figure 25. STRESSES IN Y - DIRECTION

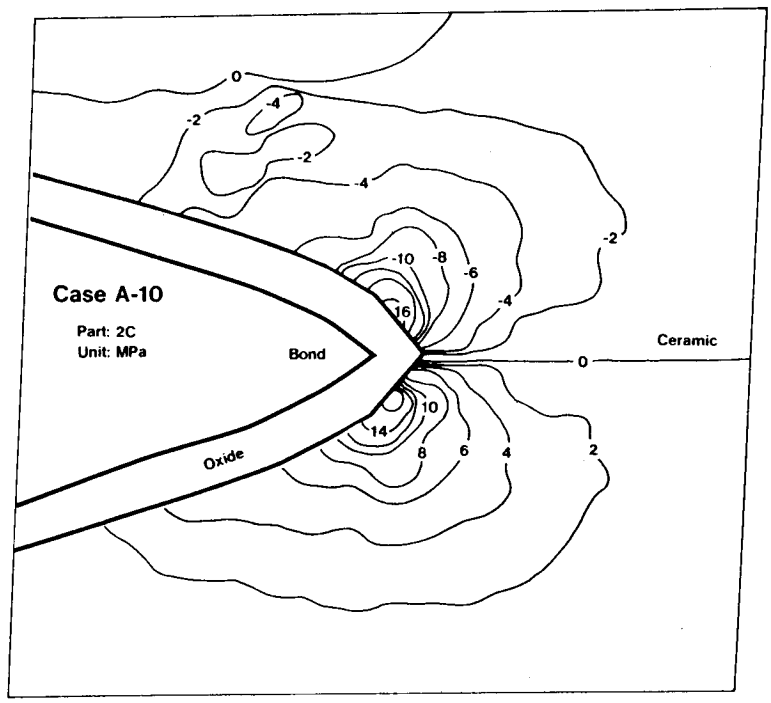

Figure 26. SHEARING STRESSES

PROPOSED MECHANISM FOR OXIDATION INDUCED THERMAL BARRIER COATING FAILURE

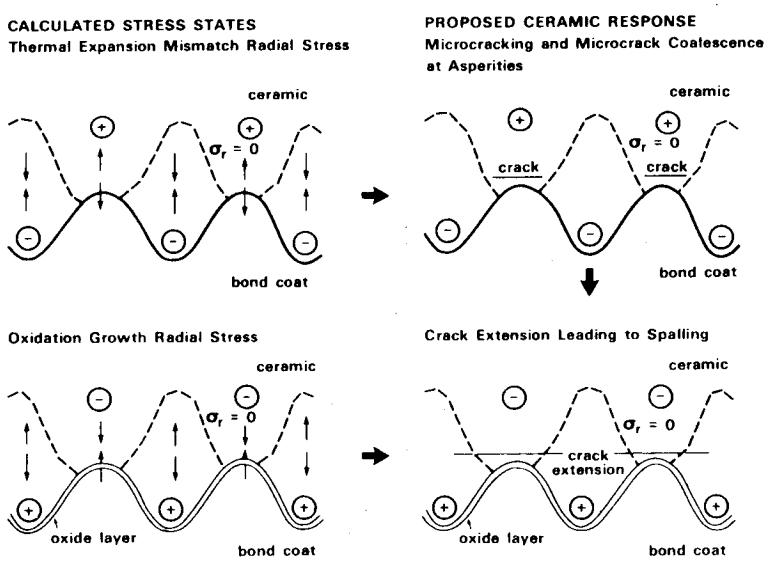

Figure 27. PROPOSED FAILURE MECHANISM